Available online at www.sciencedirect.com
SCIENCE DIRECT®
Bioorganic & Medicinal Chemistry 12 (2004) 2887–2893
Bioorganic & Medicinal Chemistry

[11C]Choline as a PET biomarker for assessment of prostate cancer tumor models

Qi-Huang Zheng,[a,*] Thomas A. Gardner,[b] Sudhanshu Raikwar,[b] Chinghai Kao,[b] K. Lee Stone,[a] Tanya D. Martinez,[a] Bruce H. Mock,[a] Xiangshu Fei,[a] Ji-Quan Wang[a] and Gary D. Hutchins[a]

[a]*Department of Radiology, Indiana University School of Medicine, 1345 West 16th Street, L-3 Room 202, Indianapolis, IN 46202-2111, USA*
[b]*Department of Urology, Indiana University School of Medicine, 975 West Walnut Street, Indianapolis, IN 46202-5121, USA*

Received 1 October 2003; accepted 17 March 2004
Available online 27 April 2004

Abstract—[11C]Choline has been evaluated as a positron emission tomography (PET) biomarker for assessment of established human prostate cancer tumor models. [11C]Choline was prepared by the reaction of [11C]methyl triflate with 2-dimethylaminoethanol (DMAE) and isolated and purified by solid-phase extraction (SPE) method in 60–85% yield based on [11C]CO_2, 15–20 min overall synthesis time from end of bombardment (EOB), 95–99% radiochemical purity and specific activity >0.8 Ci/μmol at end of synthesis (EOS). The biodistribution of [11C]choline was determined at 30 min post iv injection in prostate cancer tumor models C4-2, PC-3, CWR22rv, and LNCaP tumor-bearing athymic mice. The results showed the accumulation of [11C]choline in these tumors was 1.0% dose/g in C4-2 mouse, 0.4% dose/g in PC-3 mice, 3.2% dose/g in CWR22rv mice, and 1.4% dose/g in LNCaP mice; the ratios of tumor/muscle (T/M) and tumor/blood (T/B) were 2.3 (T/M, C4-2), 1.4 (T/M, PC-3), 2.5 (T/M, CWR22rv), 1.2 (T/M, LNCaP) and 2.6 (T/B, C4-2), 2.6 (T/B, PC-3), 7.8 (T/B, CWR22rv), 3.2 (T/B, LNCaP), respectively. The micro-PET imaging of [11C]choline in prostate cancer tumor models was acquired from a C4-2, PC-3, CWR22rv, or LNCaP implanted mouse at 30 min post iv injection of 1 mCi of the tracer using a dedicated high resolution (<3 mm full-width at half-maximum) small FOV (field-of-view) PET imaging system, IndyPET-II scanner, developed in our laboratory, which showed the accumulation of [11C]choline in C4-2, PC-3, CWR22rv, or LNCaP tumor implanted in a nude athymic mouse. The initial dynamic micro-PET imaging data indicated the average T/M ratios were approximately 3.0 (C4-2), 2.1 (PC-3), 3.5 (CWR22rv), and 3.3 (LNCaP), respectively, which showed the tumor accumulation of [11C]choline in all four tumor models is high. These results suggest that there are significant differences in [11C]choline accumulation between these different tumor types, and these differences might offer some useful measure of tumor biological process.

1. Introduction

Prostate cancer is the most commonly diagnosed cancer and is the second leading cause of cancer death in men over the age 40 in the United States.[1] According to estimates, about 220,900 American men would be diagnosed with prostate cancer in the year of 2003 and 28,900 men would die from this disease. Detection of prostate cancer by various imaging methods is vital to overall management and treatment of prostate cancer patients. Biomedical imaging technique positron emission tomography (PET) coupled with appropriate radiopharmaceuticals has become a clinically valuable and accepted diagnostic tool to image prostate cancer.[2] PET has been widely used in the diagnosis and staging of primary tumors, detection of subclinical disease, assessment of therapy response, and detection of recurrence.[3]

The most widely used radiopharmaceutical for studies in oncology is [18F]-2-fluoro-2-deoxyglucose (FDG). FDG is the only PET cancer imaging agent used clinically. FDG has been reported to be an effective imaging agent for the detection of primary and metastatic prostate cancer. FDG-PET has been used successfully in an

* Corresponding author. Tel.: +1-317-278-4671; fax: +1-317-278-9711; e-mail: qzheng@iupui.edu

0968-0896/$ - see front matter © 2004 Elsevier Ltd. All rights reserved.
doi:10.1016/j.bmc.2004.03.051

increasing number of oncological applications and is considered a valuable adjunct to anatomic imaging methods, providing unique functional information for better characterization of disease.[4] FDG has shown promise in predicting outcomes and detecting prostate tumors based on metabolic activity of the tumor(s); however, the low cellular uptake rate of FDG in prostate cancer limits its usefulness, and several other radiopharmaceuticals have been developed that evaluate prostate tumors based on other physiologic properties. For example, [^{11}C]choline has been used as a PET tracer for human cancer detection and succeeded in visualizing prostate cancer and many other types of cancers in patients.[5–8] [^{18}F]Fluorocholine and F-18 labeled choline analogues also have been developed as new and promising oncologic PET tracers for prostate cancer and breast cancer in human.[9–11] However, the mechanism of the choline accumulation in tumors is not clear. The concept of [^{11}C]choline as an oncologic PET tracer has been reported as follows. An elevated level of phosphatidylcholine has been revealed in tumors, which is the most abundant phospholipid in the cell membranes of all eukaryotic cells and provides a potential target for tumor imaging. This elevation is thought as the result of increased uptake of choline, a precursor of the biosynthesis of phosphatidylcholine.[5] Thus, [^{11}C]choline, [^{18}F]fluorocholine, and F-18 labeled choline analogues can be used as PET biomarkers for imaging choline kinase in cell membranes in cancers, and [^{11}C]choline and [^{18}F]fluorocholine have been found clinically useful in humans for the study of prostate cancer.

PET has been used clinically to measure enzyme reactions, ligand–receptor interactions, cellular metabolism, and cell proliferation. Until recently, however, PET has not been suitable for small animal models because of resolution limitations.[12,13] In an effort to develop novel prostate cancer biomarkers for molecular imaging,[14] a series of PET cancer imaging agents that target either receptors or enzymes have been synthesized in this laboratory.[15–22] In an effort to develop micro-PET instrumentation for small and intermediate sized animals imaging applications, high-resolution, high-sensitivity dedicated research scanners, IndyPET and IndyPET-II, have been designed and characterized by the same laboratory.[23,24] Development of micro-PET instrumentation for small animal imaging and the availability of positron-emitting tracers have made this technology accessible for the noninvasive, quantitative, and repetitive imaging of biological function in living animals. Because small animal PET is immediately extrapolated to the clinic, laboratory advances should rapidly be translated to clinical practice.[12] To the best of our knowledge, the [^{11}C]choline study of the prostate cancer animal models is still not reported in the literature. We have used [^{11}C]choline-PET for imaging of breast cancer animal models,[25] and we extrapolated whether [^{11}C]choline might be able to assess prostate cancer tumor models using micro-PET in vivo. In this paper, we evaluate the behavior of [^{11}C]choline in four established human prostate cancer tumor models C4-2, PC-3, CWR22rv, and LNCaP tumor-bearing athymic mice.

2. Results and discussion

2.1. Synthesis of [^{11}C]choline

[^{11}C]Choline was prepared by the reaction of [^{11}C]methyl triflate[26] with 2-dimethylaminoethanol (DMAE) and isolated and purified by solid-phase extraction (SPE) method[27,28] in 60–85% yield based on [^{11}C]CO_2, 15–20 min overall synthesis time from end of bombardment (EOB), 95–99% radiochemical purity, and specific activity >0.8 Ci/μmol at end of synthesis (EOS). [^{11}C]Choline was synthesized before by others using very similar chemistry.[6,8,29,30] The difference in the present paper is that [^{11}C]methyl triflate is used instead of [^{11}C]methyl iodide, in which [^{11}C]methyl triflate is a proven methylation reagent with greater reactivity than [^{11}C]methyl iodide.[31] A simple home-built technique[32] for convenient labeling and isolation of [^{11}C]-methyl]quaternary amines by N-^{11}C-methylation method was employed in the radiosynthesis of [^{11}C]choline. The quality control (QC) process to determine the radiochemical purity of [^{11}C]choline and the quantity of DMAE in the final product was performed using HPLC methods. The UV-detector we used did have the detection threshold for DMAE, and we did establish the retention time of DMAE, however, the chromatogram obtained from the HPLC system that we utilized did not show the peak of DMAE in the final [^{11}C]choline solution. It was therefore impossible to determine accurately the quantity of DMAE in the final product. The published QC data for the concentration of DMAE in the final solution were 9–13 ppm using two separate reverse phase HPLC methods[33] and 6.9 ppm using cation-exchange chromatography,[30] which employed the same SPE technique for the [^{11}C]choline synthesis. The final solution of [^{11}C]choline with low concentration of starting material we prepared is suitable for injection in animals.

2.2. Prostate cancer tumor models

The prostate cancer tumor models we used were the human prostate cancer/athymice mouse xenograft models implanted with several popular human prostate cancer cell lines C4-2, PC-3, CWR22rv, and LNCaP. LNCaP, an androgen-responsive, androgen receptor (AR) positive, prostate-specific antigen (PSA) secreting human prostate cancer cell line, was derived from a cervical lymph node metastasis by Horoszewicz et al.[34] It serves as a parental cell line. C4-2 is a hormone-refractory derivative of the LNCaP epithelial prostate cancer cell line that was derived by passing through castrated mice and remains AR- and PSA-positive.[35,36] PC-3 is an androgen-independent (AI), AR-, and PSA-negative human prostate cancer cell line established by Kaighn et al.[37] from the bone marrow aspirates of a patient with confirmed metastatic disease. CWR22rv is one of the more recently developed transplantable human prostate tumor models.[38,39] This tumor exhibits androgen-dependent growth and PSA secretion in male nude athymic mice and regresses in response to androgen withdrawal. The CWR22rv cell line is a valuable

tool for studying prostate cancer progression to a hormone-refractory state, because it possesses features of clinical advanced disease: AR expression, AI proliferation, and androgen-responsiveness. It serves as a model possessing an intermediate, or transition, phenotype between that of hormone-sensitive, AR-positive cell lines (e.g., LNCaP) and AI-, AR-negative cell lines (e.g., PC-3).[40] These models have proven to be useful and become popular for investigations of human prostate cancer.

2.3. In vivo biodistribution of [^{11}C]choline in tumor models

In vivo biodistribution data of [^{11}C]choline in C4-2, PC-3, CWR22rv, and LNCaP tumor cell lines implanted athymic mice are indicated in Table 1. Since it was difficult to generate C4-2 tumor model, we only had one C4-2 tumor-bearing mouse for the biodistribution study. The data presented here for PC-3 and CWR22rv tumor-bearing mice represented the average value in three mice, and the data presented here for LNCaP tumor-bearing mice represented the average value in five mice. The average values were taken not only over several mice, but also over the several tumors in each mouse. In C4-2, PC-3, CWR22rv, and LNCaP tumor-bearing athymic mice, the liver and kidneys were found to show very high accumulation of [^{11}C]choline, consistent with findings using [^{18}F]fluorocholine in CWR22rv and PC-3 xenografts.[10,41] In comparison with heart, liver, lungs, spleen, kidneys, and small intestine, biodistribution studies of [^{11}C]choline in four prostate cancer tumor models did not show higher accumulation in tumors than in other tissues; and in comparison with blood, brain, bone, and muscle, biodistribution studies of [^{11}C]choline in four prostate cancer tumor models did show higher accumulation in tumors than in other tissues. The ratios of tumor/muscle (T/M) and tumor/blood (T/B) may serve as the important parameters to guide in vivo evaluation of [^{11}C]choline as a PET biomarker in prostate cancer tumor models. In general, the higher T/M and T/B ratios will show the higher tumor accumulation of tracer in biodistribution studies, and tumors will be more visible with the tracer in micro-PET imaging studies. In order to be able to claim that the tumor accumulation of the tracer is high, the lower threshold for T/M and T/B ratios should be set at least more than 1.[17] The biodistribution study results of T/M and T/B ratios presented here are very similar or superior to the reported findings using [^{18}F]FDG (T/M: 1.4; T/B: 4.4) and [^{11}C]acetate (T/M: 1.5; T/B: 2.2) in CWR22rv xenograft.[42] The biodistribution data are similar in LNCaP and C4-2 mice, and different in PC-3 and CWR22rv mice, since the biological properties between LNCaP tumor and C4-2 tumor are similar, and the biological properties between LNCaP, C4-2 tumors and PC-3 tumor and CWR22rv tumor are different. These results suggest the differences in radioactivity retention in tumors might be in relation to biological differences between these various cell lines.

2.4. IndyPET-II scanner

The animal PET scanners, IndyPET and IndyPET-II, were designed and developed by Hutchins and co-workers.[23,24] These are high resolution (<3 mm full-width at half-maximum), high sensitivity, research PET scanner developed for small field-of-view (FOV) imaging applications including rodent imaging (mice and rats), intermediate size animals (dogs, pigs, and primates), and dedicated human imaging applications (brain, breast). The micro-PET scanner we used is IndyPET-II scanner.

2.5. In vivo micro-PET imaging of [^{11}C]choline in tumor models

Tumor-specific micro-PET imaging was performed using the IndyPET-II scanner for 15 min static scans after an initial 30 min accumulation period of [^{11}C]choline. In vivo micro-PET images of [^{11}C]choline in C4-2, PC-3, CWR22rv, and LNCaP tumors implanted in a nude athymic mouse are shown in Figure 1. The PET images show a lot of accumulation of the tracer in the liver. The regions of the tumor are difficult to decipher from the images, because the activity spilling over from the liver might result in overestimation of tumor accumulation. The tracer retention in C4-2 tumor mouse and

Table 1. Biodistribution data (% dose/g) of [^{11}C]choline in C4-2, PC-3, CWR22rv, and LNCaP prostate tumor-bearing athymic mice at 30 min post iv injection

Tissue	C4-2 ($n = 1$)	PC-3 ($n = 3$)	CWR22rv ($n = 3$)	LNCaP ($n = 5$)
Blood	0.39	0.19 ± 0.12	0.49 ± 0.31	0.45 ± 0.26
Brain	0.64	0.16 ± 0.02	0.64 ± 0.31	0.45 ± 0.25
Heart	2.21	1.06 ± 0.35	4.32 ± 1.44	5.28 ± 3.06
Liver	14.16	9.07 ± 3.65	23.31 ± 6.52	14.93 ± 10.12
Lungs	3.99	1.23 ± 0.21	5.95 ± 1.96	4.60 ± 2.90
Spleen	1.84	1.28 ± 0.49	5.43 ± 1.94	2.93 ± 1.49
Kidneys	13.16	5.12 ± 1.76	14.90 ± 5.62	17.23 ± 9.11
Small intestine	2.02	1.94 ± 0.52	6.55 ± 2.02	4.67 ± 2.25
Bone	0.69	0.44 ± 0.12	1.46 ± 0.71	1.12 ± 0.68
Muscle	0.45	0.31 ± 0.12	1.46 ± 0.80	1.18 ± 0.64
Tumor	1.02	0.44 ± 0.17	3.16 ± 0.71	1.36 ± 0.68
Tumor/muscle ratio	2.27	1.42 ± 0.23	2.47 ± 0.98	1.17 ± 0.36
Tumor/blood ratio	2.62	2.55 ± 0.63	7.79 ± 3.50	3.19 ± 0.82

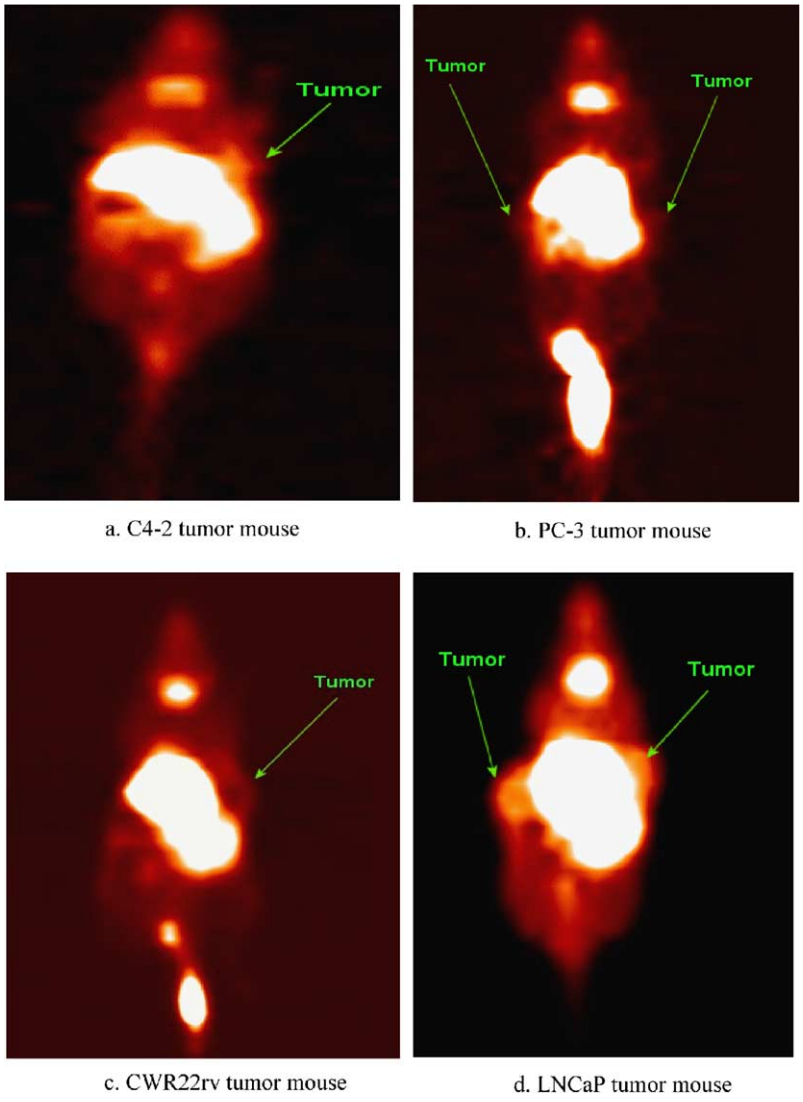

Figure 1. Micro-PET images of [^{11}C]choline in a C4-2 (a), PC-3 (b), CWR22rv (c), and LNCaP (d) tumor-bearing athymic mouse.

LNCaP tumor mouse is clear, and the C4-2 tumor and LNCaP tumor in micro-PET images are visible. The tracer retention in PC-3 tumor mouse and CWR22rv tumor mouse in micro-PET images is unclear, which is not consistent with their biodistribution data.

In order to quantitate PET data, the initial dynamic micro-PET imaging studies were performed in C4-2, PC-3, CWR22rv, and LNCaP tumor-bearing mice. The time activity curves for T/M ratios versus time are shown in Figure 2 (a. C4-2 tumor; b. PC-3 tumors; c. CWR22rv tumor; d. LNCaP tumors) with the average T/M ratio at an approximate value 3.0 (C4-2), 2.1 (PC-3), 3.5 (CWR22rv), and 3.3 (LNCaP), respectively. The T/M ratio found from dynamic PET data is systematically much higher than that from biodistribution data. A region of interest (ROI) was placed on the organ or tumor of interest in the transaxial micro-PET images that include the entire organ or tumor volume. The average radioactivity concentration within a tumor or an organ was obtained from the average pixel values within the multiple ROI volume.[42] The T/M ratio data showed the tumor retention of [^{11}C]choline in all four prostate cancer tumor models is high. T/M is more or less constant over the whole time period. This is also the case for T and M or both were increasing or decreasing at a same rate. Figure 2 demonstrated both the differences in reproducibility between tumor types and the obvious differences in kinetics between tumors. These differences are correlative with both the biodistribution data and the cell biology of the various tumor lines. In particular, the tumors with the highest overall accumulation of radioactivity (CWR22rv tumor, 3.16% dose/g) also had the more protracted uptake phase. This is also the similar case in LNCaP tumor (1.36% dose/g). It is likely the highest overall retention of radioactivity in tumors would accumulate more slowly. The dynamic IndyPET-II data are similar in LNCaP and C4-2 mice, and different in PC-3 and CWR22rv mice, because the cell biology between LNCaP tumor and C4-2 tumor are similar, and the cell biology between LNCaP, C4-2 tumors and PC-3 tumor and CWR22rv tumor are differ-

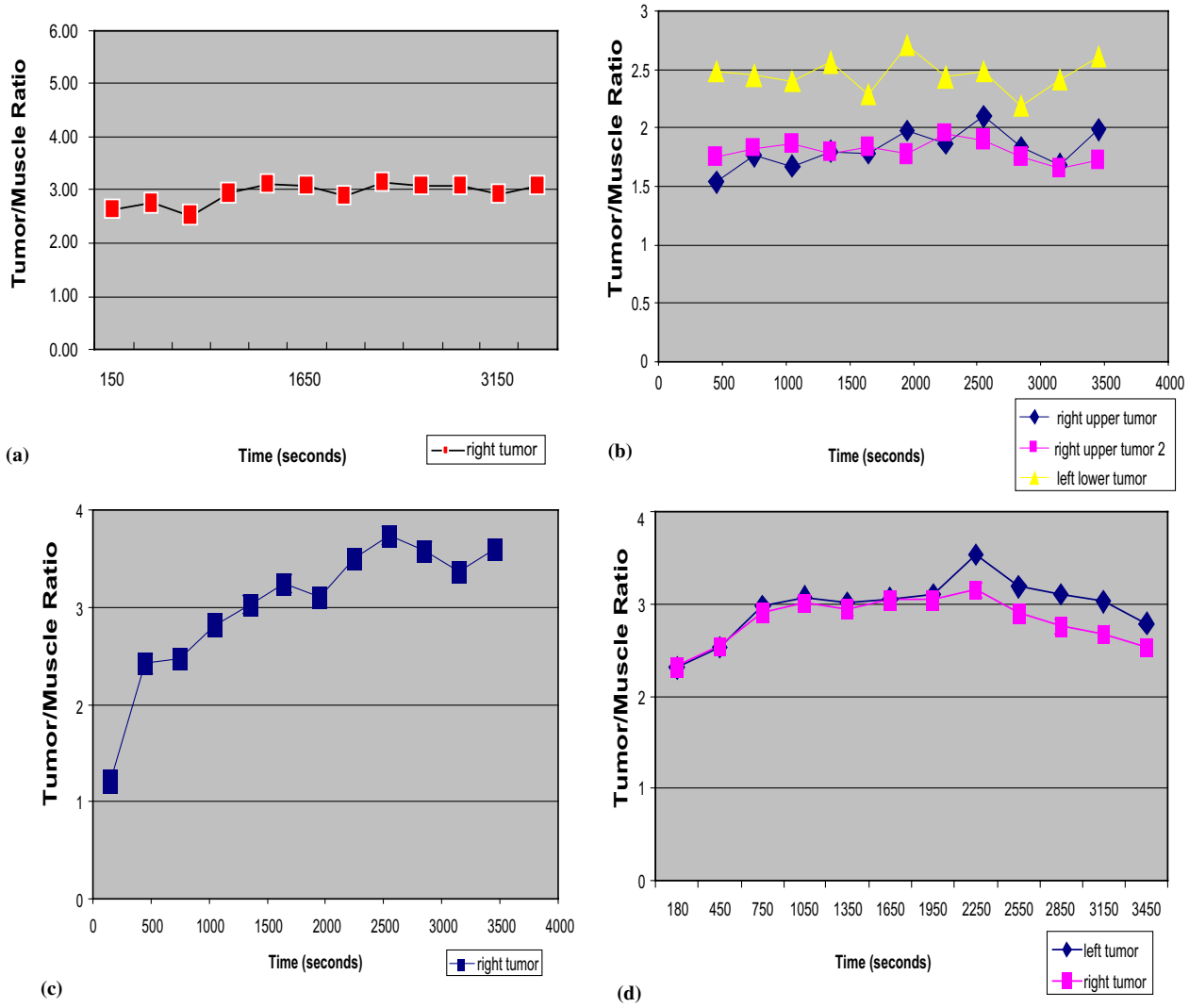

Figure 2. Tumor/muscle ratio versus time curve in C4-2 (a), PC-3 (b), CWR22rv (c), and LNCaP (d) tumors, the average tumor/muscle ratios are approximately 3.0, 2.1, 3.5, and 3.3, respectively.

ent. These results suggest the kinetic differences in radioactivity accumulation in tumors might be in relation to cell biology differences between these various cell lines.

It is interesting to note that the tumor/muscle ratios of biodistribution studies are lower than the micro-PET derived ratios in all the four models. This is unusual and the opposite finding (i.e., lower ratios by micro-PET may have been expected). This might suggest that the ROI's in PET images need to be carefully examined. With the IndyPET-II scanner, a mouse study had a quantitative accuracy of less than 10% in error, and most within the 5% range, regardless of whether the ROI is superficial or deep within the mouse body. The partial volume effect in estimating the ROI values from micro-PET images were small in these IndyPET-II scans because the resolution of the IndyPET-II scanner is around 2.5 mm and the implanted prostate tumors were in the range of 1 cm or more than 1 cm in diameter, which was well above the resolution limit of this animal PET system. Moreover, the dynamic IndyPET-II imaging studies were co-registered with the EVS RS-9 micro-CT imaging studies,[43] which helped to select and draw ROI. Therefore, we conclude the dynamic IndyPET-II data are more reliable and less partial volume effects were involved. However, the discrepancy between biodistribution and micro-PET data need to be further studied.

3. Conclusion

In summary, we have developed a simple technique for the radiosynthesis and routine production of [^{11}C]choline. In vivo biodistribution studies and in vivo micro-PET images of [^{11}C]choline in prostate cancer athymic mice showed that [^{11}C]choline had different accumulation with C4-2, PC-3, CWR22rv, and LNCaP tumors. These results suggest that there are significant differences in [^{11}C]choline accumulation between these different tumor types, and these differences might offer some useful measure of tumor biological process.

4. Materials and methods

4.1. General

All commercial reagents and solvents were used without further purification. The [^{11}C]methyl triflate was made according to the literature procedures[26,31] by the metathetical reaction of [^{11}C]methyl bromide over a hot column of silver triflate supported on porous graphite. One silver triflate column was used for 20–40 [^{11}C]methyl triflate runs before replacement.

Analytical HPLC was performed using a Prodigy (Phenomenex) 5 μm C-18 column, 4.6×250 mm; 3:1:3 CH_3CN/MeOH/20 mM, pH 6.7 $KHPO_4^-$ mobile phase, flow rate 1.5 mL/min, and UV (240 nm) and γ-ray (NaI) flow detectors. Semi-prep C-18 SiO_2 Sep-Pak type cartridges were obtained from Waters Corporation, Milford, MA. Sterile vented Millex-GS 0.22 μm vented filter units were obtained from Millipore Corporation, Bedford, MA.

4.2. Synthesis of [^{11}C]choline

The precursor 2-dimethylaminoethanol (10 μL) was dissolved in acetonitrile (250 μL). The mixture was transferred to a small volume, three-neck reaction tube. [^{11}C]Methyl triflate was passed into the air-cooled reaction tube at −15 to −20 °C, which was generated by a Venturi cooling device powered with 100 psi compressed air, until activity reaches a maximum (2–3 min), then the reaction tube was isolated and heated at 70–80 °C for 2–3 min. The reaction tube was connected to the SiO_2 Sep-Pak type cartridge. The product solution was passed onto the Sep-Pak cartridge for solid-phase extraction (SPE) by gas pressure. The reaction tube and Sep-Pak were washed with ethanol (2×5 mL), and the washing solution was discarded to a waste bottle. The product was eluted from the Sep-Pak with 90:8:2 H_2O/EtOH/HOAc (4.6 mL) and sterile-filtered through a 0.22 μm cellulose acetate membrane and collected into a sterile vial. The pH was adjusted to 5.5–7.0 with 2 M NaOH and 150 mM NaH_2PO_4 mixed solution (1:20, ~0.4 mL). Total radioactivity was assayed and the total volume was noted. The overall synthesis time was 15–20 min. The decay-corrected yield, from $^{11}CO_2$, was 60–85%, and the radiochemical purity was 95–99% by analytical HPLC method. Retention times in the analytical HPLC system we utilized were 2.0 min for [^{11}C]choline and 2.4 min for DMAE.

4.3. Prostate cancer athymic mice

All animal experiments were performed under a protocol approved by the Indiana University institutional animal care and use committee. Six weeks old male, athymic nude mice (Harlan) were used for the generation of subcutaneous prostate tumor xenografts. For the generation of C4-2 and LNCaP models, 10 million cells (per injection site per animal) in the log phase were gently mixed with 100 μL of ice cold Matrigel (Becton-Dickinson Biosciences) and injected in the lower flank region of the mouse using a 27 gauge 1/2 cc syringe. For generating PC-3 tumors 2 million cells/injection site per animal were used without any Matrigel. CWR22rv tumors were generated by injecting 5 million cells in the presence of Matrigel per injection site per animal. Palpable tumors became evident within 4–8 weeks post-implantation. The size of the palpable tumors was in the range of 1 cm or more than 1 cm in diameter. The tumors were firm without necrotic tissue around the tumors. The tumor sizes varied between the different models.

4.4. Biodistribution studies of [^{11}C]choline in prostate cancer athymic mice

Athymic mice 8 weeks post-xenograft implantation were injected intravenously with sub-pharmacologic doses (1–3 mCi) of [^{11}C]choline via the tail vein while under conscious restraint. At 30 min post injection, mice were sacrificed by decapitation under halothane anesthesia, their tissues quickly excised, weighed, and the decay-corrected radioactive content measured using an auto Packard Cobra Quantum gamma counter. The tissue localization at 30 min time point, expressed as % of injected dose per gram of tissue (% dose/g), weight normalized % dose/g and % of injected dose per organ were calculated from the tissue count and weight data using an Excel spreadsheet program.

4.5. Micro-PET imaging of [^{11}C]choline in prostate cancer athymic mice

The IndyPET-II scanner was used for these studies. The mouse was anesthetized with acepromazine (0.2 mg/kg, i.m.) and torbugesic (0.2 mg/kg, i.m.). One millicurie of [^{11}C]choline was administered intravenously to the mouse in tail vein. The micro-PET imaging of [^{11}C]choline in prostate cancer athymic mice was acquired by the ordered subsets expectation maximization (OSEM) using six subsets/four iterations for 5 min from a C4-2, PC-3, CWR22rv, or LNCaP tumor-bearing mouse at 30 min post iv injection of 1 mCi of the tracer. Dynamic imaging was performed for 60 min starting at the injection of 1 mCi of [^{11}C]choline to each mouse. The frame durations were defined as 300 s for entire 3600 s scan. All images were acquired in list-mode and sorted into 15×20 s frames, 10×60 s frames, and 9×300 s frames. Images were reconstructed using filtered back projection with a 70% Hanning filter (4.242 cm^{-1} cutoff frequency).

Acknowledgements

This work was partially supported by the Susan G. Komen Breast Cancer Foundation grant IMG 02-1550 (to QHZ), the Department of Defense Congressionally Directed Medical Research Programs grant DAMD17-03-1-0077 (to TAG), the National Institutes of Health/

National Cancer Institute grant P20CA86350 (to G.D.H.), the Indiana 21st Century Research and Technology Fund (to G.D.H.), and the Lilly Endowment Inc. (to the Indiana Genomics Initiative (INGEN) of Indiana University). Many helpful criticisms and comments from the reviewers and editor for the revision of the manuscript are greatly appreciated.

References and notes

1. Jemal, A.; Thomas, A.; Murray, T.; Thun, M. *CA Cancer J. Clin.* **2002**, *52*, 23.
2. Jadvar, H.; Pinski, J. K.; Conti, P. S. *Oncol. Rep.* **2003**, *10*, 1485.
3. Varagnolo, L.; Stokkel, M. P. M.; Mazzi, U.; Pauwels, E. K. J. *Nucl. Med. Biol.* **2000**, *27*, 103.
4. Smith, D. A. T. *Nucl. Med. Commun.* **1998**, *19*, 97.
5. Hara, T.; Kosaka, N.; Kishi, H. *J. Nucl. Med.* **1998**, *39*, 990.
6. Hara, T.; Kosaka, N.; Shinoura, N.; Kondo, T. *J. Nucl. Med.* **1997**, *38*, 842.
7. Hara, T.; Kosaka, N.; Kishi, H.; Kobori, O. *J. Nucl. Med.* **1997**, *38*, 250P.
8. Hara, T.; Yuasa, M. *Appl. Radiat. Isot.* **1999**, *50*, 531.
9. DeGrado, T. R.; Baldwin, S. W.; Wang, S.; Orr, M. D.; Liao, R. P.; Friedman, H. S.; Reiman, R.; Price, D. T.; Coleman, R. E. *J. Nucl. Med.* **2001**, *42*, 1805.
10. DeGrado, T. R.; Coleman, R. E.; Wang, S.; Baldwin, S. W.; Orr, M. D.; Robertson, C. N.; Polascik, T. J.; Price, D. T. *Cancer Res.* **2000**, *61*, 110.
11. DeGrado, T. R.; Reiman, R. E.; Price, D. T.; Wang, S.; Coleman, R. E. *J. Nucl. Med.* **2002**, *43*, 92.
12. Herschman, H. R. *Curr. Opin. Immunol.* **2003**, *15*, 378.
13. Del Guerra, A.; Belcari, N. *Q. J. Nucl. Med.* **2002**, *46*, 35.
14. Weissleder, R.; Mahmood, U. *Radiology* **2001**, *219*, 316.
15. Fei, X.; Zheng, Q.-H.; Hutchins, G. D.; Liu, X.; Stone, K. L.; Carlson, K. A.; Mock, B. H.; Winkle, W. L.; Glick-Wilson, B. E.; Miller, K. D.; Fife, R. S.; Sledge, G. W.; Sun, H. B.; Carr, R. E. *J. Label. Compd. Radiopharm.* **2002**, *45*, 449.
16. Zheng, Q.-H.; Fei, X.; Liu, X.; Wang, J.-Q.; Sun, H. B.; Mock, B. H.; Stone, K. L.; Martinez, T. D.; Miller, K. D.; Sledge, G. W.; Hutchins, G. D. *Nucl. Med. Biol.* **2002**, *29*, 761.
17. Zheng, Q.-H.; Fei, X.; DeGrado, T. R.; Wang, J.-Q.; Stone, K. L.; Martinez, T. D.; Gay, D. J.; Baity, W. L.; Mock, B. H.; Glick-Wilson, B. E.; Sullivan, M. L.; Miller, K. D.; Sledge, G. W.; Hutchins, G. D. *Nucl. Med. Biol.* **2003**, *30*, 753.
18. Liu, X.; Zheng, Q.-H.; Fei, X.; Wang, J.-Q.; Ohannesian, D. W.; Erickson, L. C.; Stone, K. L.; Hutchins, G. D. *Bioorg. Med. Chem. Lett.* **2003**, *13*, 641.
19. Zheng, Q.-H.; Liu, X.; Fei, X.; Wang, J.-Q.; Ohannesian, D. W.; Erickson, L. C.; Stone, K. L.; Hutchins, G. D. *Nucl. Med. Biol.* **2003**, *30*, 405.
20. Wang, J.-Q.; Zheng, Q.-H.; Fei, X.; Liu, X.; Gardner, T. A.; Kao, C.; Raikwar, S. P.; Glick-Wilson, B. E.; Sullivan, M. L.; Mock, B. H.; Hutchins, G. D. *Synth. Commun.* **2004**, *34*, 917.
21. Zheng, Q.-H.; Wang, J.-Q.; Liu, X.; Fei, X.; Mock, B. H.; Glick-Wilson, B. E.; Sullivan, M. L.; Raikwar, S. P.; Gardner, T. A.; Kao, C.; Hutchins, G. D. *Synth. Commun.* **2004**, *34*, 689.
22. Zheng, Q.-H.; Wang, J.-Q.; Fei, X.; Hutchins, G. D. *Synthesis* **2003**;(18), 2785.
23. Frese, T.; Rouze, N. C.; Bouman, C. A.; Sauer, K.; Hutchins, G. D. *IEEE Trans. Med. Imaging* **2003**, *22*, 258.
24. Rouze, N. C.; Hutchins, G. D. *IEEE Trans. Nucl. Sci.* **2003**, *50*, 1491.
25. Zheng, Q.-H.; Stone, K. L.; Mock, B. H.; Miller, K. D.; Fei, X.; Liu, X.; Wang, J.-Q.; Glick-Wilson, B. E.; Sledge, G. W.; Hutchins, G. D. *Nucl. Med. Biol.* **2002**, *29*, 803.
26. Mock, B. H.; Mulholland, G. K.; Vavrek, M. T. *Nucl. Med. Biol.* **1999**, *26*, 467.
27. Zheng, Q.-H.; Mulholland, G. K. *Nucl. Med. Biol.* **1996**, *23*, 981.
28. Mulholland, G. K.; Zheng, Q.-H.; Mock, B. H.; Vavrek, M. T. *J. Label. Compd. Radiopharm.* **1999**, *42*, S459.
29. Pascali, C.; Bogni, A.; Iwata, R.; Cambie, M.; Bombardieri, E. *J. Label. Compd. Radiopharm.* **2000**, *43*, 195.
30. Mishani, E.; Ben-David, I.; Rozen, Y. *Nucl. Med. Biol.* **2002**, *29*, 359.
31. Jewett, D. M. *Appl. Radiat. Isot.* **1992**, *43*, 1383.
32. Zheng, Q.-H.; Liu, X.; Fei, X.; Wang, J.-Q.; Mock, B. H.; Glick-Wilson, B. E.; Sullivan, M. L.; Hutchins, G. D. *Bioorg. Med. Chem. Lett.* **2003**, *13*, 1787.
33. Mishani, E.; Bocher, M.; Ben-David, I.; Rozen, Y.; Laky, D.; Marciano, R.; Chisin, R. *J. Label. Compd. Radiopharm.* **2001**, *44*, S379.
34. Horoszewicz, J. S.; Leong, S. S.; Kawinski, E.; Karr, J. P.; Rosenthal, H.; Chu, T. M.; Mirand, E. A.; Murphy, G. P. *Cancer Res.* **1983**, *43*, 1809.
35. Wu, H. C.; Hsieh, J. T.; Gleave, M. E.; Brown, N. M.; Pathak, S.; Chung, L. W. *Int. J. Cancer* **1994**, *57*, 406.
36. Matsubara, S.; Wada, Y.; Gardner, T. A.; Egawa, M.; Park, M. S.; Hsieh, C. L.; Zhau, H. E.; Kao, C.; Kamidono, S.; Gillenwater, J. Y.; Chung, L. W. *Cancer Res.* **2001**, *61*, 6012.
37. Kaighn, M. E.; Narayan, K. S.; Ohnuki, Y.; Lechner, J. F.; Jones, L. W. *Invest. Urol.* **1979**, *17*, 16.
38. Pretlow, T. G.; Wolman, S. R.; Micale, M. A.; Pelley, R. J.; Kursh, E. D.; Resnick, M. I.; Bodner, D. R.; Jacobberger, J. W.; Delmoro, C. M.; Giaconia, J. M. *J. Natl. Cancer Inst.* **1993**, *85*, 394.
39. Wainstein, M. A.; He, F.; Robinson, D.; Kung, H. J.; Schwartz, S.; Giaconia, J. M.; Edgehouse, N. L.; Pretlow, T. P.; Bodner, D. R.; Kursh, E. D. *Cancer Res.* **1994**, *54*, 6049.
40. Tepper, C. G.; Boucher, D. L.; Ryan, P. E.; Ma, A. H.; Xia, L.; Lee, L. F.; Pretlow, T. G.; Kung, H. J. *Cancer Res.* **2002**, *62*, 6606.
41. Price, D. T.; Coleman, R. E.; Liao, R. P.; Robertson, C. N.; Polascik, T. J.; DeGrado, T. R. *J. Urol.* **2002**, *168*, 273.
42. Oyama, N.; Kim, J.; Jones, L. A.; Mercer, N. M.; Engelbach, J. A.; Sharp, T. L.; Welch, M. *J. Nucl. Med. Biol.* **2002**, *29*, 783.
43. Hutchins, G. D.; Rouze, N.; Stone, K. L.; Krishnamurthi, G.; Liang, Y. J. *Nucl. Med.* **2002**, *43*, 59P.